XII International Conference on Computational Plasticity. Fundamentals and Applications
COMPLAS XII
E. Oñate, D.R.J. Owen, D. Peric and B. Suárez (Eds)

A FINITE ELEMENT METHOD FOR THERMO-MECHANICAL COUPLING ANALYSIS OF SHAPE MEMORY ALLOYS

H. Ahmadian*† and S. Mohammadi†

† High Performance Computing Laboratory (HPC Lab)
School of Civil Engineering
University of Tehran, Tehran, Iran
e-mail: h.ahmadian@ut.ac.ir , web page: http://chpc.ut.ac.ir/

Keywords: Shape memory alloy, thermo-mechanical coupling, finite element.

Abstract. Due to strong thermo-mechanical coupling in shape memory alloys (SMAs), heat generation/absorption during forward/reverse phase transformation can cause temperature variations in the material; influencing its mechanical behaviour. It is usually assumed that this coupling is only affected by the loading rate. But, recently studies have shown that the size of the structure and the boundary conditions are also important. Therefore, only the definition of quasi-static or slow loading rate can not guarantee an isothermal process and so further considerations need to be made.

Based on the powerful model, proposed by Lagoudas et al. [1] and later improved for computer programming using the return mapping algorithm by Qidwai and Lagoudas [2], this contribution presents a three-dimensional thermo-mechanically coupled extension which describes two important typical phenomena of material model of SMAs: superelasticity and superplasticity (shape memory effect). An algorithm is then proposed to implement the coupled model into a finite element code. Performed simulations with different boundary conditions demonstrate that the both loading rate and the size dependency can be captured within the proposed framework. The results are in good agreement with available data in the literature.

1 INTRODUCTION

Shape memory alloys (SMAs) are the type of smart materials that have been used in a variety of applications from damping devices in civil engineering to micro-actuators in MEMS technology. An interesting characteristics of these materials is that they can undergo large deformations and recover from it through temperature changes (shape memory effect or super-plasticity) or stress changes (pseudo-elasticity or super-elasticity). In typical temperature regimes, SMAs show two phases with different properties; One is the high temperature phase called austenite (A) and the other is the low temperature phase called martensite (M). The phase transformation between these two phases forms the basis of the unique behavior of SMAs.

It is well known that phase transformation in SMAs is exothermal during the forward transformation (A to M) and endothermal during the reverse transformation (M to A). This means that the temperature of SMA can increase/decrease during the forward/reverse transformation. In most available studies it has been assumed that this complicated thermo-mechanically coupled behavior is only affected by the strain rate or in general, the loading rate. But recently, it has been observed experimentally and analytically that the size of the SMA device and the boundary conditions (hence the environment that the device is placed in) are also important [3,4].

Based on the powerful model, proposed by Lagoudas *et al*. (1996) [1], this contribution presents a three-dimensional thermo-mechanically coupled extension, using a staggered algorithm in which the original problem is decoupled into two problems. In each step, first the mechanical problem is solved isothermally and then the temperature variations due to phase transformation are taken into account by solving the heat equation and this iterative procedure continues until the problem converges.

2 CONSTITUTIVE MODEL

In this section, the constitutive model of [2] is discussed briefly. The explicit form of the Gibbs free energy is given by:

$$\begin{aligned} G(\boldsymbol{\sigma},T,\xi,\varepsilon^{th}) = &-\frac{1}{2\rho}\boldsymbol{\sigma}:\boldsymbol{S}:\boldsymbol{\sigma}-\frac{1}{\rho}\boldsymbol{\sigma}:\left[\boldsymbol{\alpha}(T-T_0)+\varepsilon^t\right] \\ &+c\left[(T-T_0)-T\ln\left(\frac{T}{T_0}\right)\right]-s_0T+u_0+\frac{1}{\rho}f(\xi) \end{aligned} \tag{1}$$

where the material parameters $\boldsymbol{S},\boldsymbol{\alpha},\rho,c,s_0$ and u_0 are the fourth-order effective compliance tensor, the second-order effective thermal expansion tensor, the density, the effective specific heat, the effective specific entropy at the reference state, and the effective specific internal energy at the reference state, respectively. The state variables $\boldsymbol{\sigma},\varepsilon^t,\xi,T,T_0$ are the Cauchy stress, the transformation strain, the martensitic volume fraction, the temperature and the reference temperature, respectively. The function $f(\xi)$ in (1) stands for the transformation hardening due

to phase interaction. The effective material properties of the SMA phase is determined using the rule of mixtures:

$$\begin{aligned}
\boldsymbol{S}(\xi) &= \boldsymbol{S}^{A} + \xi(\boldsymbol{S}^{M} - \boldsymbol{S}^{A}) = \boldsymbol{S}^{A} + \xi\Delta\boldsymbol{S} \\
\boldsymbol{\alpha}(\xi) &= \boldsymbol{\alpha}^{A} + \xi(\boldsymbol{\alpha}^{M} - \boldsymbol{\alpha}^{A}) = \boldsymbol{\alpha}^{A} + \xi\Delta\boldsymbol{\alpha} \\
c(\xi) &= c^{A} + \xi(c^{M} - c^{A}) = c^{A} + \xi\Delta c \\
s_0(\xi) &= s_0{}^{A} + \xi(s_0{}^{M} - s_0{}^{A}) = s_0{}^{A} + \xi\Delta s_0 \\
u_0(\xi) &= u_0{}^{A} + \xi(u_0{}^{M} - u_0{}^{A}) = u_0{}^{A} + \xi\Delta u_0
\end{aligned} \tag{2}$$

where superscripts A and M denote the austenitic and martensitic phases, respectively and Δ is the difference of a specific property between the two phases. The elastic behavior of each phase is assumed to be isotropic and linear. Note that the martensitic volume fraction ξ is an internal state variable and needs to be determined at each time increment. After substitution of the Gibbs free energy (1) into the first and second laws of thermodynamics, the constitutive relation for the total strain is given by:

$$\varepsilon = -\rho\frac{\partial G}{\partial \boldsymbol{\sigma}} = \boldsymbol{S} : \boldsymbol{\sigma} + \boldsymbol{\alpha}(T - T_0) + \varepsilon^{t} \tag{3}$$

The flow rule of the incremental constitutive model or the relation between the evolution of transformation strain tensor and evolution of martensitic volume fraction can be defined as:

$$\dot{\varepsilon}^{t} = \Lambda\dot{\xi} \tag{4}$$

where Λ , is the transformation tensor,

$$\Lambda = \begin{cases} \dfrac{3}{2}H\dfrac{\sigma'}{\sqrt{\dfrac{3}{2}\left\|\sigma'\right\|^{2}}} \; ; & \dot{\xi} > 0 \\ H\dfrac{\varepsilon^{t-R}}{\sqrt{\dfrac{2}{3}\left\|\varepsilon^{t-R}\right\|^{2}}} \; ; & \dot{\xi} < 0 \end{cases} \tag{5}$$

where H is the material parameter associated with the maximum uniaxial transformation strain. σ' is the deviatoric stress tensor and ε^{t-R} is the transformation strain at the reversal point. The constitutive relations are numerically solved by an implicit scheme based on the classical return mapping plasticity and the Newton-Raphson method. Detail of the implementation can be found in [2].

3 THERMOMECHANICAL COUPLING

In this section the discrete form of heat equation of SMAs is discussed. The fully coupled form of the heat equation of SMAs is given by [5]:

$$T\alpha : \dot{\sigma} + \rho c \dot{T} + (-\pi + T\Delta\alpha : \sigma - \rho\Delta c \ln(\frac{T}{T_0}) + \rho\Delta s_0 T)\dot{\xi} = -\nabla . q \tag{6}$$

where π is the thermodynamic force,

$$\pi = \sigma : \Lambda - \rho \frac{\partial G}{\partial \xi} \tag{7}$$

The first term of the left-hand side of (6) expresses how the temperature changes due to a change in the stress, while the second term of the left-hand side is related to the heat capacity. The third term of the left-hand side expresses how the temperature of SMA changes due to a variation of the martensitic volume fraction. The term on the right-hand side of (6) is related to the heat transfer process by the heat flux q.

Using the Fourier's law of heat conduction, $q = -k\nabla T$, and assuming that the thermal conductivity, the effective specific heat and the thermal expansion coefficient of the two phases are identical (which is true for most of SMAs), the heat equation yields:

$$T\alpha : \dot{\sigma} + \rho c \dot{T} + (-\pi + \rho\Delta s_0 T)\dot{\xi} = \nabla . (k\nabla T) \tag{8}$$

The boundary conditions need to be imposed. In general boundary conditions are of convection type,

$$q.n = -(k\nabla T).n = h(T - T_{ext}) \tag{9}$$

where h is the convection coefficient, n is the outgoing perpendicular vector and T_{ext} is the external temperature. Temperature distributions at $t = 0$ is given as the initial condition $T = T_{ext}$.

After conventional finite element discretization, the heat equation (8) can be compacted to an ordinary differential equation,

$$(K + K_h + K_\sigma + K_\xi).T + M.\dot{T} = F \tag{10}$$

or in an incremental form:

$$(K + K_h + K_\sigma^{n+1} + K_\xi^{n+1}).T^{n+1} + M.\frac{T^{n+1} - T^n}{\Delta t} = F^{n+1} \tag{11}$$

Where the superscript n is the index of the increment, Δt is the time of each increment, K is the heat conduction matrix, K_h is the heat convection matrix, K_σ is the matrix of latent heat due

to stress changes, K_ξ is the matrix of latent heat due to martensite volume fraction changes, M is the heat capacity matrix and F is an imaginary load vector,

$$
\begin{aligned}
(K)_{ij} &= \int_\Omega k \nabla N_i \nabla N_j \, d\Omega \\
(K_h)_{ij} &= \int_S h N_i N_j \, dS \\
(K_\sigma)_{ij} &= \int_\Omega \alpha : \dot{\sigma} N_i N_j d\Omega \\
(K_\xi)_{ij} &= \int_\Omega \rho \Delta s_0 \dot{\xi} N_i N_j d\Omega \\
(M)_{ij} &= \int_\Omega \rho c N_i N_j \, d\Omega \\
(F)_i &= \int_S h T_{ext} N_i \, dS + \int_\Omega \pi \dot{\xi} N_i d\Omega
\end{aligned}
\tag{12}
$$

where N_i, N_j are the finite element shape functions. Ultimately, the temperature at the increment $n+1$ is given as:

$$
\begin{aligned}
T^{n+1} &= (K_{im}{}^{n+1})^{-1} \, (F_{im}{}^{n+1}) \\
K_{im}{}^{n+1} &= (K + K_h + K_\sigma{}^{n+1} + K_\xi{}^{n+1} + \frac{M}{\Delta t}) \\
F_{im}{}^{n+1} &= (F^{n+1} + \frac{M}{\Delta t} T^n)
\end{aligned}
\tag{13}
$$

where K_{im} and F_{im} are imaginary stiffness matrix and force vector, respectively.

4 NUMERICAL RESULTS

In the first simulation, the model is assessed by simulating different rates of loading-unloading in a pseudo-elasticity experimental problem, previously reported by [6]. Unfortunately, in [6] some of the required material parameters of the present model were not reported. Instead, several uniaxial tension tests are available with clear results of the stress and strain values at the start and completion of transformation, which can be used for calibrating the model [2]. The adopted material properties are listed in Table 1. The tests are carried out on a thin strip with $30\,mm$ length, $2.6\,mm$ width and $0.5\,mm$ thickness, which is fixed at both ends and is elongated till a given strain of 0.08 under the displacement control condition. The ambient and initial temperatures are equal to $23°C$. The original experiments were conducted in air, but we provide the results of simulations in air and water to discuss the substantial effect of convective boundary conditions on the material response. Therefore, a common value of $50\ W/(m^2K)$ for the average

convection coefficient in air and $800\ W/(m^2K)$ in water is chosen [7]. The conduction coefficient of $18 W/(m\,K)$ is adopted for $Ni_{50}Ti_{50}$ [5].

Table 1: SMA Material Properties

E_M	$16.5\times10^9\ Pa$	$\alpha_A=\alpha_M$	$22\times10^{-6}1/K$
E_A	$16.5\times10^9\ Pa$	$\rho c_A=\rho c_M$	$3.2\times10^5\ J/(m^3K)$
$\nu_A=\nu_M$	0.3	$\rho\Delta s_0$	$-0.375\times10^6\ J/(m^3\ K^1)$
M_s	$-30°C$	H_{max}	0.05
M_f	$-31°C$	k	$18\ W/(m\,K)$
A_s	$4°C$	h_{Air}	$50\ W/(m^2K)$
A_f	$5°C$	h_{Water}	$800\ W/(m^2K)$

The stress-strain curves at different strain rates of 1.1×10^{-1}, 1.1×10^{-2}, 1.1×10^{-3} and 1.1×10^{-4} are presented in Figures 1.a-d, for both the experimental data and numerical simulations. Clearly, the performed simulations in air are in excellent agreement with the experimental data, with only a difference at the onset of forward phase transformation. This region represents the nucleation phenomenon that shows itself in the global response as a stress peak. This phenomenon is a consequence of unstable phase transformation and strain softening at local level. Often an SMA element is cyclically trained to shake out this initial unstable behavior [8]. In this study, however simulations are confined to the stable behavior. At the low strain rate of 1.1×10^{-4}, there is an excellent agreement with the experimental data. By the of the increase the strain rate to 1.1×10^{-3} and further 1.1×10^{-2}, the curves tend to deviate from each other during the reverse transformation. In addition to the nucleation phenomenon, the high heat exchange between the specimen and the grips can force the temperature of the material to decrease faster during the unloading, causing higher slopes of the reverse phase transformation plateau. But at the near adiabatic condition strain rate of 1.1×10^{-1}, the specimen would not have enough time to dissipate the latent heat to the environment. Consequently, at this strain rate, slopes of the reverse transformation plateau in the experiment and numerical simulation become nearly identical.

Since at intermediate strain rates such as $1.1\times10^{-3}s^{-1}$, the amount of heat exchange with the environment due to convection is comparable to the amount of latent heat generation/ absorption due to the forward/reverse transformation, a slightly nonlinear behavior can be observed in the transformation region of stress-strain curves at this strain rate. With increasing or decreasing the strain rate, the heat generation/absorption or heat exchange will become dominant. Either way, the transformation region of the stress-strain would become nearly linear. Therefore, the material behavior of SMAs at different strain rates can be characterized by a competition between the heat exchange and internal heat generation or absorption during the phase change [9].

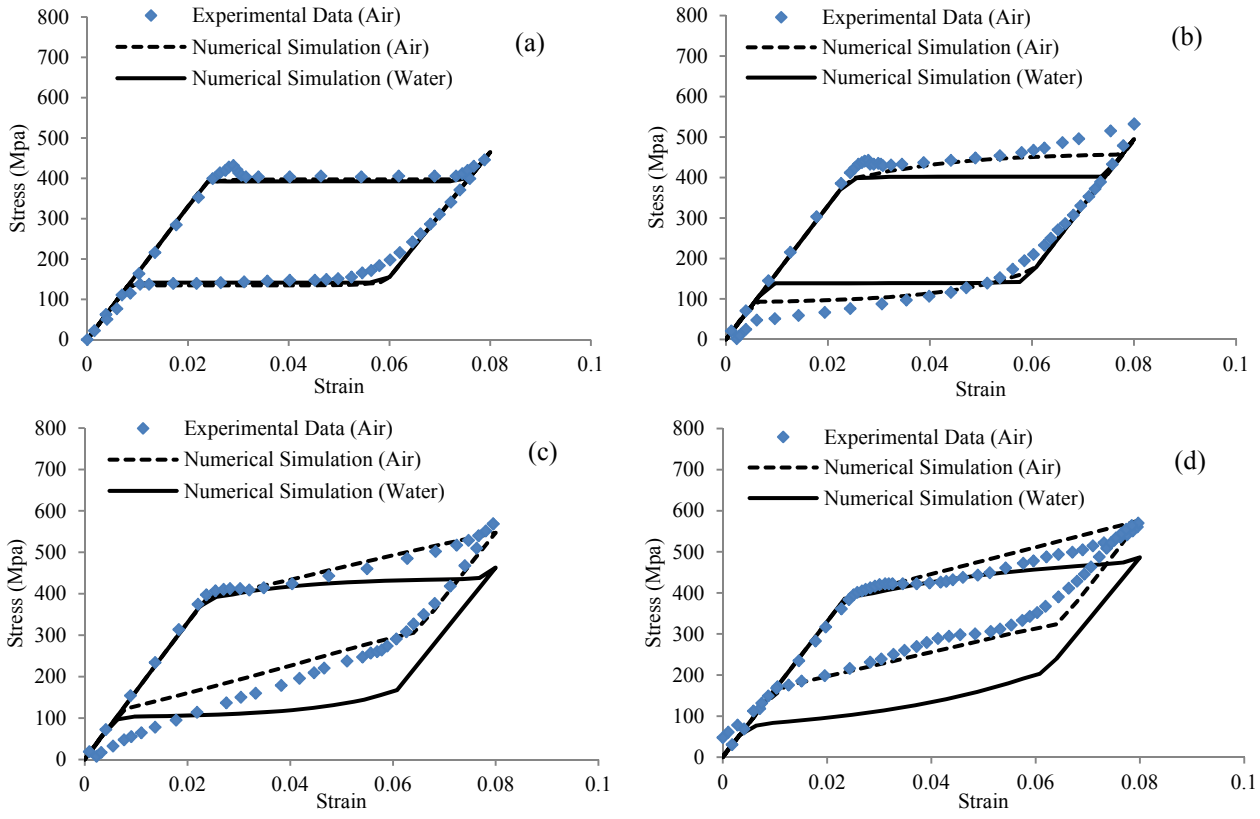

Figure 1: Comparison of the experimental and numerical simulation for the strain rate of (a) $1.1\times10^{-4}\,s^{-1}$, (b) $1.1\times10^{-3}\,s^{-1}$, (c) $1.1\times10^{-2}\,s^{-1}$ and (d) $1.1\times10^{-1}\,s^{-1}$.

The effect of convective boundary conditions is also studied in Figures 1.a-d. For this purpose, simulations are performed in water which has a higher value of convection coefficient which means higher heat exchange with the environment. As shown in Figures 1.a-d, by increasing the convection coefficient, the slope of the stress-strain curve decreases and therefore a near-isothermal material response of SMAs in highly convective environment such as water is expected.

Now, all simulations are performed in air. During the forward transformation, the temperature of the material increases monotonically with an increasing strain rate, resulting in higher stress levels as can be seen in Figure 2. During the reverse transformation, however, increasing the strain rate does not necessarily lead to lower stress levels (see lower stress plateaus in Figure 2). As it can be seen in Figure 3, the stress level of reverse transformation is decreased with increasing the strain rate to approximately the strain rate of $1.1\times10^{-2}\,s^{-1}$. However, further increase in the strain rate causes the reverse transformation stress level to increase. The reason can be attributed to the fact that at these strain rates, the released latent heat does not have enough

time to transfer to the environment completely. So, at the start of the reverse transformation, the temperature of the material becomes much higher than the ambient temperature, leading to higher stress levels. Consequently, the temperature of the material may become higher or lower than or even equal to the ambient temperature after the unloading depending on the value of strain rate.

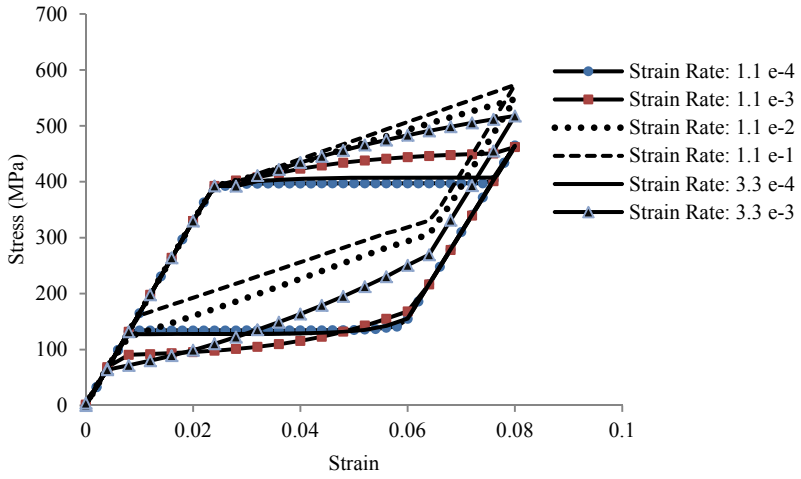

Figure 2: Numerical stress-strain curves for different strain rates

As mentioned earlier, the size of an SMA device plays an important role on its response. The reason can be attributed to the fact that the heat transfer in regions near the boundary is different from that in the centerline, which can cause a temperature non-uniformity in the cross section. Because of strong thermo-mechanical coupling this non-uniformity causes non-uniform stress distribution and therefore non-uniform phase transformation in the cross section. This effect can be ignored for devices with small dimensions such as thin wires. But it is quite important for larger devices such as the SMA plates used to control buckling or post-buckling in the structural control field. For this purpose, numerical simulations are performed at a constant nearly low strain rate of 1.1×10^{-3} on three thin strips with different length/width ratios of $100, 10$ and 2 which are fixed at both ends and are elongated till a given strain of 0.095 under the displacement control condition. Problems are solved using a plane-stress finite element model. Temperature is fixed at right and left side of the structure and is equal to $23°C$. Material properties are the same as previous example.

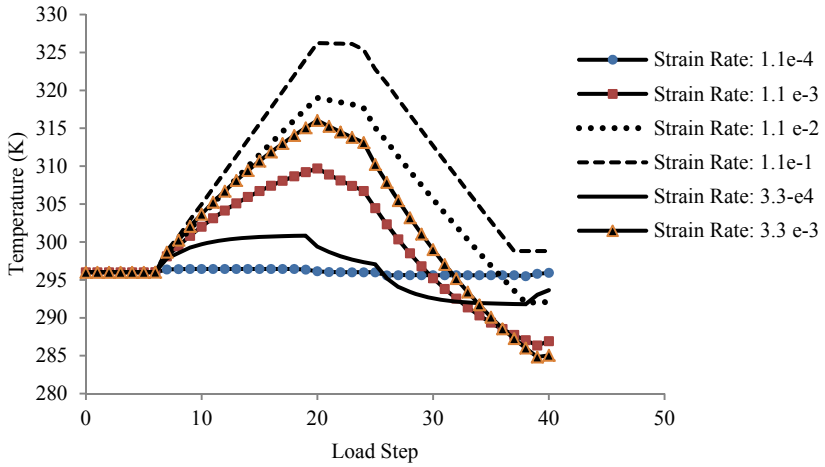

Figure 3: Numerical temperature variations-load steps for different strain rates

The global stress- strain responses for different length/width ratios are presented in Figure 4. During forward transformation, the material response changes from nearly isothermal to nearly adiabatic condition by the change of length/width ratio. This phenomenon can be explained by the non-uniformity of temperature which causes the temperature to be much higher, at inner regions compared to outer regions near the boundary. As the size of the device increases, the temperature of the inner regions increases. Therefore, the overall material response experiences higher stress levels. To explain the non-monotonic stress level changes during the reverse transformation, a similar discussion such as the one made on Figure 2, can be applied.

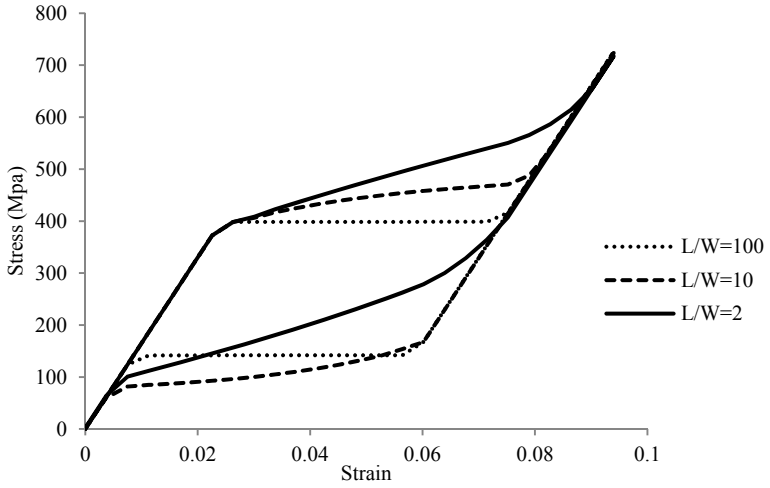

Figure 4: Global stress-strain responses of three SMA devices

5 CONCLUSION

In this contribution, a finite element framework for coupled thermo-mechanical problems in SMAs is presented. The present formulation is capable of simulating 3D thermo-mechanically coupled response of SMAs in various ambient and boundary conditions. Several numerical simulations are performed to understand the underlying concept of thermo-mechanical coupling in SMAs and some are compared with available experimental data to evaluate the accuracy of the model. It has been observed that the slow strain rate can not guarantee an isothermal process and some other variables need to be considered to be ensured of material response with an acceptable accuracy.

6 REFERENCES

[1] Lagoudas, D.C. Bo, Z. and Qidwai, M.A. A unified thermodynamic constitutive model for SMA and finite element analysis of active metal matrix composites. *Mech. Compos. Mater. Struct.* (1996) **3**:153-179.

[2] Qidwai, M.A. and Lagoudas, D.C. Numerical implementation of shape memory alloy thermomechanical constitutive model using return mapping algorithms. *Int. J. Num. Meth. Engng.* (2000) **47**:1123-1168.

[3] DesRoches, R. McCormick, J. and Delemont, M. Cyclic properties of superelastic shape memory alloy wires and bars. *J. Struct. Eng.* (2004) **130**(1):38-46.

[4] Mirzaeifar, R. DesRoches, R. and Yavari, A. Analysis of the rate-dependent coupled thermo-mechanical response of shape memory alloy bars and wires in tension. *Continuum Mech. Thermodyn.* (2011) **23**:363-385.

[5] Lagoudas, D.C. *Shape memory alloy, modeling and engineering applications*. Springer, (2008).

[6] Zhang, X.H. Feng, P. He, Y.J. Yu, T.X. and Sun, Q.P. Experimental study on rate dependence of macroscopic domain and stress hysteresis in NiTi shape memory alloy strips. *Int. J. Mech. Sci.* (2010) **52**:1660-1670.

[7] Morin, C. Moumni, Z. and Zaki, W. A constitutive model for shape memory alloys accounting for thermomechanical coupling. *Int. J. Plast.* (2011) **27**:748-767.

[8] Iadicola, M. and Shaw, J. Rate and thermal sensitivities of unstable transformation behavior in a shape memory alloy. *Int. J. Plast.* (2004) **20**:577-605.

[9] He, Y.J. and Sun, Q.P. On non-monotonic rate dependence of stress hysteresis of superelastic shape memory alloy bars. *Int. J. Solids. Struct.* (2011) **48**:1688-1695.